Validation of a Motion Sickness Prediction Model via Flight Tests on DLR's Bo-105 Helicopter

Philippe Petit*
Research Engineer
Institute of Flight Systems DLR (German Aerospace Center), Brunswick, Germany

In previous work, a motion sickness prediction model aimed at vertical lift applications was developed. To validate this model, flight tests with an MBB Bo-105 Helicopter owned and operated by the DLR were conducted. In total, 32 test subjects were flown in 16 sorties on 30 min sinusoidal flight paths of various frequencies. The test design and implementation included the development of a suitable measurement flight instrumentation, auditive cueing systems for accurate following of the test trajectory, and questionnaires for recording motion sickness during flight. The results are analyzed, and it is shown that the previously developed motion sickness prediction model agrees well with the motion sickness observed during flight in the case of medium motion sickness.

Introduction

Motion sickness (also known as kinetosis) can be induced by various means, including railway travel (Ref. 1), ship travel (Ref. 2), car travel (Ref. 3), or air travel (Ref. 4). Even motion simulators (Ref. 5) can provoke motion sickness. Symptoms include nausea, vomiting, cold sweat, headache, sleepiness, yawning, loss of appetite, and increased salivation, which also conveys the idea that motion sickness is generally not a desirable state. In the recent past, it has been identified that motion sickness is a noteworthy topic for some forms of transport, most prominently perhaps, the railway transport where the introduction of tilting trains promoted the study of this topic. Especially in countries where high-speed trains are introduced to curvy tracks, motion sickness becomes a problem among passengers as has been shown by Förstberg et al. (Ref. 1). Furthermore, it can be easily seen that a similar problem arises for modern transport solutions. One such problem could be the introduction of self-driving cars and therefore the simultaneous rise of self-driving carsickness as examined by Diels and Bos (Ref. 6). If we extrapolate these arguments for the upcoming technology of urban air transport as proposed by numerous startups and companies, it is easily imaginable that motion sickness poses a serious problem for this kind of transport, especially if considering the proposed air taxis, which will most likely travel at low altitude over dense urban airspace in conjuncture with many other air taxis. Such operational conditions will not only generate fairly complex movement patterns but are also prone to atmospheric disturbances like gusts. Given these circumstances, we predict that motion sickness will play a substantial role in the adoption of such urban air mobility concepts. People certainly will not be excited about a transport solution which is faster but makes them sick every time it is used. Therefore, the following research question arises: How can motion sickness be accurately predicted given a flight path or an aircraft motion of a vertical take-off and landing (VTOL) aircraft? This step is important in order to mitigate these risks in subsequent steps, for example, in the design of a flight control system. Kamiji et al. (Ref. 7) proposed a new motion sickness prediction model, which hinges on the idea of directly modeling the human motion sickness mechanism. In a previous publication by the author (Ref. 8), this prediction model was numerically optimized with the help of empirical motion sickness data gathered from literature sources in order to further enhance the prediction results. However, due to a lack of data, it could not be determined how accurate this model was in a real-life scenario. In order to fill this gap, we conducted flight tests with a small helicopter in order to gather data targeted for the validation of this motion sickness prediction model.

The following text is structured as follows: First, a short recapitulation of the improved Kamiji model, presented in Ref. 8 is given, followed by a presentation of the overall flight-test design. Furthermore, the development and implementation of the flight-test instrumentation, auditive cueing system, and questionnaires are introduced. The results of these flight tests will then be statistically analyzed and compared to the motion sickness prediction of the improved Kamiji model of Ref. 8. The paper is concluded with a conclusion and outlook.

Improved Kamiji model

In a past publication (Ref. 8), the improved Kamiji model for predicting motion sickness was presented. This model tries to explicitly model the human motion sickness mechanism based on the sensory conflict theory first developed by Reason and Brand (Ref. 9). It postulates that motion sickness arises from a conflict of sensory inputs between

*Corresponding author; email: philippe.petit@dlr.de.
Presented at the Vertical Flight Society 79th Annual Forum & Technology Display, West Palm Beach, FL, May 16–18, 2023. Manuscript received July 2023; accepted May 2024.

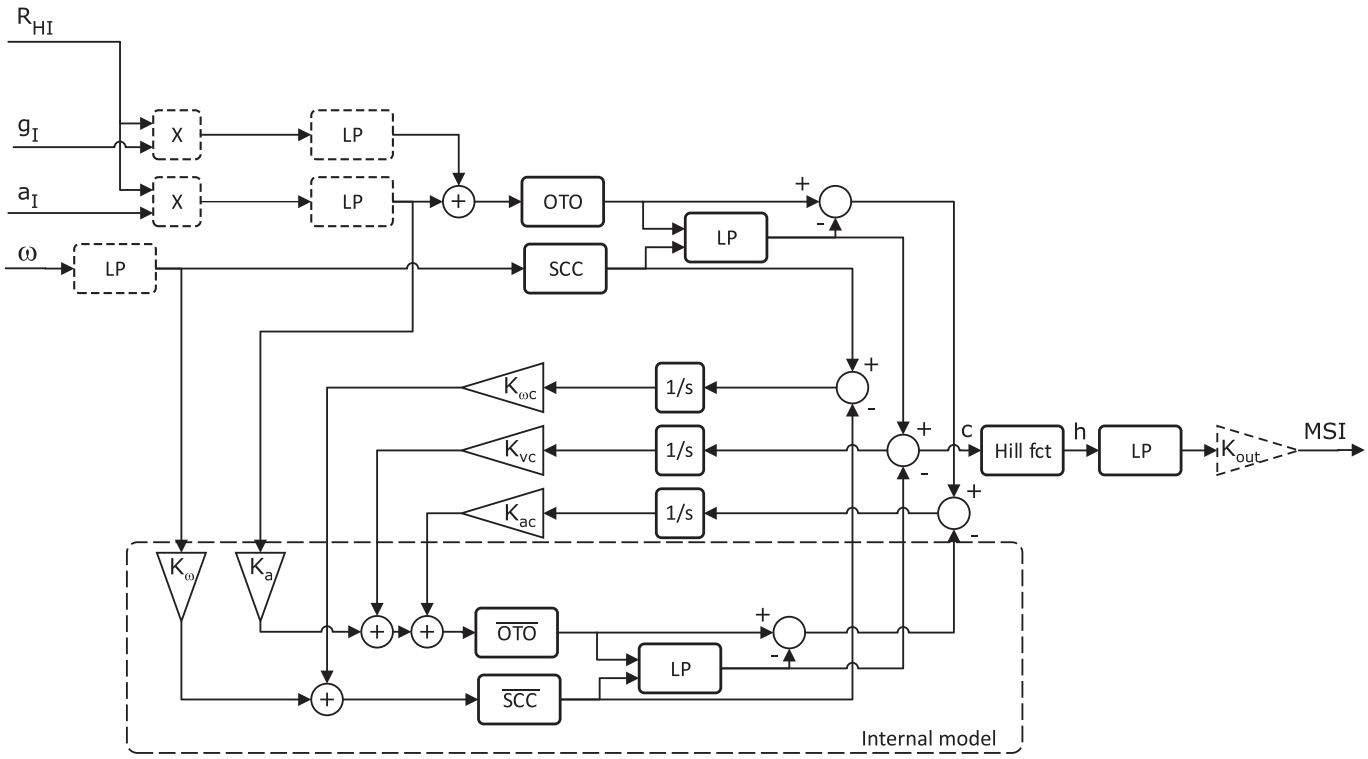

Fig. 1. Block diagram of the modified Kamiji motion sickness model as presented in Ref. 8. Newly added blocks are marked with a dashed outline.

the vestibular system (inner ear) and the eye which differs from past experience. Bos and Bles (Ref. 10) first proposed to directly simulate the sensory conflict theory and therefore to obtain a motion sickness metric from motion data in the time domain. This approach was adapted by Kamiji et al. (Ref. 7) and further improved to include 6-Degrees of Freedom (DoF) motions. This Kamiji motion sickness model was then once more improved by the author of this study in Ref. 8. For this, the structure of the model was adapted such that it complies with common aerospace standards, and the inherent parameters of the model were optimized with the help of an empirical dataset taken from the literature. The final block-diagram structure is depicted in Fig. 1. Again, the idea behind the Kamiji motion sickness model is to explicitly model the motion sickness conflict. Therefore, given an inertial acceleration a_I and inertial gravitational force g_I, rotational rates ω as well as the transformation matrix R_{HI} from inertial to head frame, the model shall predict the "motion sickness incidence" (MSI), or in other words, the percentage of people getting sick. As detailed by the original paper (Ref. 7), the model consists of a replication of the vestibular system which itself is comprised of the semicircular canals (SCC) as well as the otoliths (OTO), and the "internal mode" brain replica of these two blocks $\overline{\text{SCC}}$ and $\overline{\text{OTO}}$. Additionally, low-pass filter blocks (LP) with a solid outline are inserted into the model as these have been identified to be part of the signal-processing chain of the brain. In Ref. 8, additional low-pass filters marked with a dashed outline were inserted for better coherence with experimental data. All of these blocks are modeled as transfer functions. The coupling between the modeled vestibular system and the internal model is realized by three gains $K_{\omega c}$, K_{vc}, and K_{ac} in conjuncture with integrator blocks (1/s). The motion conflict (c) between the vestibular system and the internal model is fed through a Hill function block and is then accumulated inside yet another low-pass filter.

To optimize the various gains and time constant of the resulting model the so-called Griffin dataset was used. This dataset consists of a total of five different papers (Refs. 11–15), which contain empirical data and analysis of motion sickness experiments with humans, in order to better understand the effects of different motion forms on motion sickness. In total, 580 subjects completed 620 h of testing inside the 12 m Tilting and Translating Cabin setup of the Institute of Sound and Vibration Research in Southampton, UK. This simulator is capable of generating horizontal oscillation motions while simultaneously tilting or rolling the cabin. Each test subject performed 30 min of testing inside that motion simulator while he/she was subjected to one motion candidate, which typically involved a horizontal translational oscillation coupled with some degree of corresponding roll/pitch oscillation. The test subjects rated their motion sickness on a scale from 0 to 6 as listed in Table 1, whereby the experiment was aborted if a test subject indicated a motion sickness level of 6: "Moderate nausea and want to stop."

Table 1. Motion sickness scale used by Griffin et al. (Ref. 16)

0	No Symptoms
1	Any symptoms, however slight
2	Mild symptoms
3	Mild nausea
4	Mild to moderate nausea
5	Moderate nausea but can continue
6	Moderate nausea and want to stop

Using a nonlinear optimization algorithm, the parameters and gains of the improved Kamiji model as displayed in Fig. 1 were tuned by the author (Ref. 8) in order to better predict the empirical Griffin dataset. This tuning resulted in six different parameter sets, one for each motion sickness level of Table 1 as shown in Ref. 8. Each model predicts the percentage of people reaching one of the six motion sickness states

Fig. 2. DLR's MBB Bo-105 helicopter, registration sign D-HDDP.

given an input motion characterized by its acceleration, angular velocities, and attitude. Furthermore, the original and improved Kamiji models were compared. It was found that given the motions of the Griffin dataset, the improved Kamiji model would adequately predict the motion sickness levels experienced in these tests while the original Kamiji model strictly predicted too low values of motion sickness.

It was, therefore, concluded that the improved Kamiji model offered good motion sickness prediction capabilities which were not yet validated. As this research is focused on predicting motion sickness *for vertical lift vehicles* such as helicopters or the upcoming generation of urban air mobility vehicles, the natural next step was deemed to compare the improved Kamiji models to flight tests on motion sickness. To the best of the author's knowledge, no adequate flight-test data have been published yet. For this reason, it was decided to perform flight tests at DLR in support of the validation of the improved Kamiji model, which can also serve as a general database for motion sickness in vertical lift vehicles.

Flight-Test Design

The flight tests were conducted with DLR's Messerschmitt-Bölkow-Blohm (MBB) Bo-105 helicopter a light, twin-engine helicopter for two pilots and up to three passengers, as shown in Fig. 2. The flight experiment was chosen to be a continuous harmonic sinusoidal roll oscillation flown as coordinated turns at a fixed height and an airspeed of approximately 60 kt. Throughout the test, the helicopter was manually piloted with the help of an auditive cueing system, which will be described below. The choice of a sinusoid roll oscillation offers a continuous motion sickness excitation and furthermore mimics the horizontal maneuvering in which future urban VTOL vehicles are envisioned to fly in densely populated areas.

Each flight test was conducted at one of three frequencies: 0.025, 0.05, and 0.1 Hz. While the Bo-105 helicopter is capable of achieving significantly faster oscillations, preflight tests showed that it is not possible for human pilots to steer oscillations with higher frequencies with sufficient accuracy. In total, 16 flights were conducted in two test campaigns in the autumn of 2021, whereby five flights were conducted at 0.025 and 0.05 Hz and six flights at 0.1 Hz as indicated in Table 2. To limit the testing area, the sinusoidal test was divided into three 10 min oscillations, connected by a 180° turnaround curve at the end of each leg. A typical trajectory of the resulting flight path is shown in Fig. 3. Each flight test started at Brunswick airport (1), followed by a short flight to the testing area (2) at which the three 10 min sinusoidal oscillations took place (3). Between each leg, a turnaround curve (4) was executed. The flight concluded with a transition back to the airport (2) and a subsequent landing (1).

During the tests, two test pilots in the front and two test subjects in the left and right backseat were onboard the helicopter. In total, 32 test

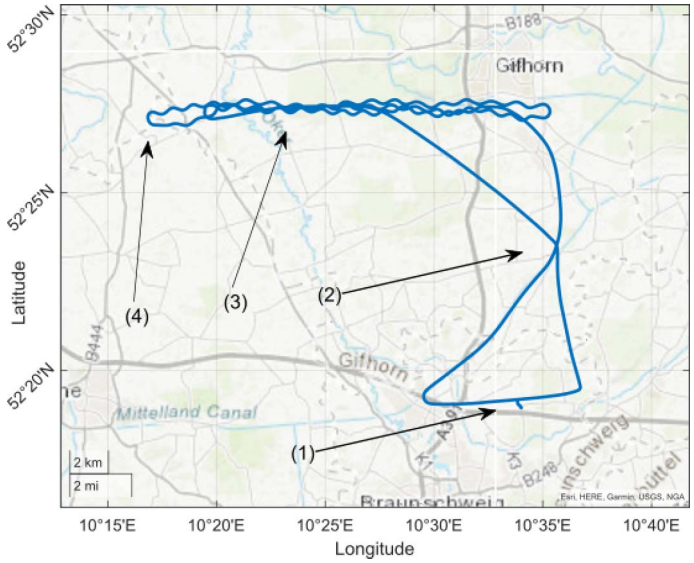

Fig. 3. The trajectory of flight test #1, representative of a typical flight test. (1): take-off/landing at Brunswick airport, (2): transit to the test track, (3): 3×10 min roll oscillation legs, (4): turnaround between experiment legs.

subjects participated in the tests with a 50–50 gender ratio. Motion sickness was indicated by the test subjects via a questionnaire, on which the test subjects would rate their subjective sickness every 2 min on the motion sickness scale Table 1 ranging from 0 to 6. If a participant indicated a motion sickness level of six, the experiment was aborted and the helicopter returned to the airport. All participants were members of the DLR in Brunswick, as no external test subjects could be taken onboard for insurance reasons. No monetary compensation was offered to the test subjects. The test subjects were instructed to take a relaxed position and look out of the window throughout the flight. Usage of electronic devices was forbidden. As the flights took place during the Covid-19 pandemic, methods for preventing infections were mandatory. All persons involved had to wear an FFP-2 mask during preflight briefing but, not during the flight test itself. Furthermore, a negative Covid-19 test was required. Overall, the flight test was designed such that it offers good comparability to the experiments of the Griffin dataset (Refs. 11–15) as it features the same experiment length, similar questionnaires, and the same motion sickness scale amongst others.

Flight-Test Instrumentation

In order to use the improved Kamiji model presented in Ref. 8, the acceleration, body rates, and orientation of the helicopter have to be recorded at a suitable frequency. This requires the presence of a flight instrumentation system capable of recording these data. Unfortunately, DLR's Bo-105 helicopter used in this experiment is not equipped with a data-recording system. For this reason, it was decided to use a hybrid approach, in which the built-in state-of-the-art Garmin G500H TXi digital multifunction display and avionics system installed on this helicopter was used in conjunction with a temporarily installed smartphone to acquire all relevant sensor data. In postprocessing data from these two sources were fused via a flight path reconstruction algorithm. This approach was first published in Ref. 17.

The advantage of combining these two sensors is that low-frequency, high-accuracy data from the installed flight display Garmin G500H TXi was fused with high-frequency, low-accuracy information of a

Table 2. Overview of performed flight tests

Flight nr.	Flight test campaign	Date	Frequency (Hz)
1	#1	September 13, 2021	0.025
2		September 13, 2021	0.05
3		September 14, 2021	0.1
4		September 14, 2021	0.025
5		September 15, 2021	0.1
6		September 16, 2021	0.025
7		September 16, 2021	0.05
8	#2	October 19, 2021	0.05
9		October 19, 2021	0.1
10		October 19, 2021	0.025
11		October 20, 2021	0.05
12		October 20, 2021	0.1
13		October 20, 2021	0.025
14		October 21, 2021	0.05
15		October 21, 2021	0.1
16		October 21, 2021	0.1

Table 3. Selected specifications of the smartphone IMU TDK/INVESENSE ICM-42632-M MEMS IMU

Characteristic	Value	Unit
	Accelerometer	
Range	±8	g
Output RMS noise	0.7	mg − RMS
Resolution	0.24	mg
Nonlinearity	±0.1	%FS
	Gyroscope	
Range	1000	°/s
Output noise	0.038	°/s − RMS
Resolution	0.03	°/s
Nonlinearity	±0.1	%FS

smartphone, resulting in a full state reconstruction of the helicopter including wind with good accuracy and high frequency of the data. The smartphone was temporarily installed by strapping it to the middle back seat with a textile rubber band. This approach has the advantage that no additional certification is required as the installation is not permanent. The data of the Garmin G500H TXi were extracted by exporting "maintenance" data onto an SD-Card *after* the flight (Ref. 18, pp. 2–38), which included lateral and normal accelerations, body rates, Euler angles, GPS positions and some other data at a rate of 1 Hz. The signal source of this display is the Garmin GSU 75H Attitude and Heading Reference System, whereby the manufacturer does not state any information on the accuracy of the datastream. The relevant certification document (Ref. 19, p. 29, 2.4.2.3.1.) details that the angles are more accurate than 1.25°; however, the standard explicitly states that no specification on angular rates or linear accelerations is given (Ref. 19, p. 4, 1.5.3).

An Android smartphone equipped with a custom application software was used to read out the sensor data of the built-in accelerometer, gyroscope, and GPS device at a rate of 500 Hz. The smartphone was selected to be a Samsung Galaxy S20 FE model featuring a Qualcomm Snapdragon 865 Octo-core processor with a clock rate of up to 2.73 GHz, six Gigabytes of RAM, and 128 Gb of internal memory as well as a 6.5-inch display which is regarded to be a medium to high-end smartphone. The built-in gyroscope/accelerometer sensor is a TDK/InvenSense ICM-42632-M Inertial Measurement Unit (IMU) featuring a triple-axis microelectromechanical systems (MEMS) gyroscope and a triple-axis MEMS accelerometer. Detailed specifications of this unit are listed in Table 3.

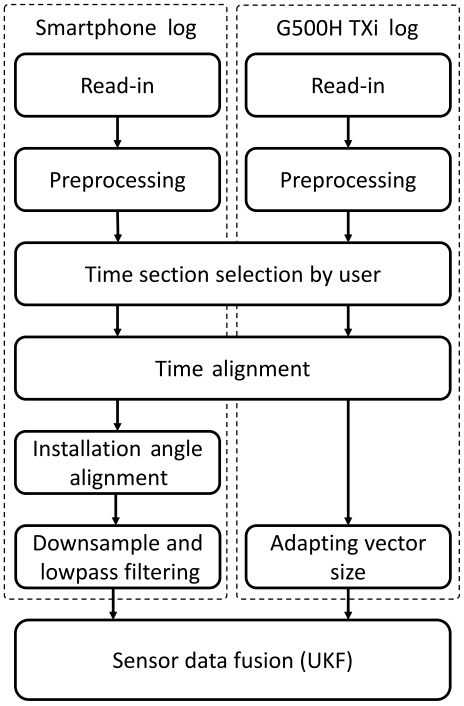

Fig. 4. Flow graph of the UKF-based data fusion.

After each flight, both datastreams were combined with the help of an unscented Kalman filter (UKF) based data fusion approach. For this, first the log files of the smartphone and Garmin G500H TXi unit were read into MATLAB®. Then the data were preprocessed which entails unit conversion, etc., followed by a time selection by the user and subsequent time alignment of both datastreams. The time alignment is based on the cross-correlation of the vertical acceleration signals of the two datastreams as these generally offer enough signal energy to accurately align the two datastreams. As the smartphone was slightly tilted as a result of its mounting on top of the rear seat, an installation angle alignment of the smartphone data had to be performed. As a last step before the data fusion could take place, the measurement vectors are inflated with empty values in the case of the Garmin data, while the smartphone data are downsampled and low-pass filtered with a cutoff frequency of 50 Hz such that both datastreams featured a sample rate of 100 Hz. A flow graph of the complete process is depicted in Fig. 4. As a last step, both sensor datastreams were fused with the help of a UKF and then smoothed with an unscented Kalman smoother as proposed in Ref. 20. The implementation was performed in MATLAB®. Large parts of the UKF and smoother implementation were taken from Ref. 21. The complete algorithm is also often called a flight path reconstruction algorithm (Ref. 21). The UKF performed in two steps. First, a rotatory UKF was executed, which fused all rotatory states of the system, with a second UKF fusing the remaining translatory states into a unified measurement vector. This approach is feasible if it is assumed that the translational and rotational accelerations are zero

$$a_x = a_y = a_z = \dot{p} = \dot{q} = \dot{r} = 0 \tag{1}$$

which corresponds to steady, unaccelerated flight. This assumption is fairly common for flight path reconstruction algorithms (Ref. 21). The resulting rotational state vector is defined as

$$\mathbf{x}_{\text{rot}} = (\dot{p}\ \dot{q}\ \dot{r}\ p\ q\ r\ \varphi\ \theta\ \psi)^T \tag{2}$$

and the corresponding state update equation

$$\dot{\mathbf{x}}_{\text{rot}} = \begin{pmatrix} 0 \\ 0 \\ 0 \\ \dot{p} \\ \dot{q} \\ \dot{r} \\ p + q\sin(\phi)\tan(\theta) + r\cos(\phi)\tan(\theta) \\ q\cos(\phi) - r\sin(\phi) \\ q\sin(\phi)\sec(\theta) + r\cos(\phi)\sec(\theta) \end{pmatrix}. \tag{3}$$

Analogously, the state vector for the translational case is given by

$$\mathbf{x}_{\text{trans}} = (a_x \;\; a_y \;\; a_z \;\; u \;\; v \;\; w \;\; x \;\; y \;\; z \;\; W_N \;\; W_E)^T \tag{4}$$

and the state update equation by

$$\dot{\mathbf{x}}_{\text{trans}} = \begin{pmatrix} 0 \\ 0 \\ 0 \\ a_x - q\cdot w + r\cdot v - g\cdot\sin(\theta) \\ a_y - r\cdot u + p\cdot w + g\cdot\sin(\phi)\cos(\theta) \\ a_z - p\cdot v + q\cdot u + g\cdot\cos(\phi)\cos(\theta) \\ R_{EB}\cdot\begin{pmatrix} u \\ v \\ w \end{pmatrix} - \begin{pmatrix} W_N \\ W_E \\ 0 \end{pmatrix} \\ 0 \\ 0 \\ 0 \\ 0 \\ 0 \end{pmatrix}. \tag{5}$$

The result of this sensor data fusion can be seen in Fig. 5.

Auditive Cueing System

As noted previously, the helicopter was tasked with performing coordinated harmonic oscillations at one of the three test frequencies. Due to the lack of an autopilot, the helicopter had to be flown manually during the entire flight test, including the experimental legs. To enable the pilot to accurately follow the required roll oscillations, an auditive cueing system was devised. In contrast to a cueing display, an auditive system has the distinct advantage of enabling the pilot to fly "eyes-out." Therefore, such a system does not interfere with the pilots normal flying duties, such as checking the instruments and observing the surroundings. The auditive cueing system indicated the desired roll oscillation by verbally announcing the desired roll angles. Therefore, the system would announce "0 *pause* 10 *pause* 20 *pause* 10 *pause* 0 *pause* −10 *pause* −20 *pause* −10 *pause* 0 etc." The timing of the callouts was chosen such that these would describe a sinusoidal curve with an amplitude of 20°. Furthermore, it could be selected which angles were announced, such that the intervals between the announcements would remain constant for different frequencies. The pilot was tasked with following and interpolating these announcements such that a smooth roll oscillation in phase with the announcements would result. This approach was first tested in a mock-up in DLR's Air Vehicle Simulator and then implemented as an iOS application, which could be loaded onto the Apple iPad digital kneeboard of the pilots. In the Bo-105 helicopter, the intercom system was used to output the audio generated by the iPad digital kneeboard and therefore could be heard via the headsets by the pilots and passengers. Pilot training for this method proved to be easy, as they quickly learned that the different callouts would serve as waypoints. For example, the pilot would know that when the "0" callout occurs, the horizon has to be level. Similarly, the "20" callout serves as a waypoint for the reversal of the oscillation. The test pilots rated the workload of this system to be high, but achievable for the 30 min duration of the flight test.

A plot of the announced and measured roll angle is displayed in Fig. 6 for the 0.025 and 0.1 Hz oscillation. It should be noted that the announced (or desired) roll angle was not included in the data logging and therefore was reconstructed and time-aligned to the measured signal via a cross-correlation approach. Therefore, no phase-shifting information can be gained from Fig. 6.

In the case of the 0.025 Hz oscillation shown in Fig. 6(b), it is evident that the pilot was able to follow the reference well. Some inconsistencies are present, especially, near the reversal points. The test pilots commented for this frequency that the oscillation was too slow for their natural steering behavior. Therefore, they were sometimes overeager to roll the helicopter back, resulting in small roll angle spikes whereby the attitude was then corrected to concur with the announcements.

For the 0.1 Hz frequency, the signal looks much cleaner although some minor overshoot can be observed. This overshoot was observed to correlate with the flight tests: The higher the frequency, the higher the overshoot of the roll angle. However, as can be seen in Fig. 6(a), even at the highest frequency of 0.1 Hz the maximum overshoot is moderate.

As can be seen in Fig. 6, the overall frequency adherence of the measured roll angle to the desired frequencies was excellent. Due to the absolute nature of the verbal cueing system, the pilot was able to accurately follow the desired roll angle, such that the resulting oscillation would be of the exact desired frequency. To confirm this fact, a Fourier analysis of each 10 min leg of all flights was performed to determine the main oscillation frequencies of each experimental leg. For the two segments shown in Figs. 6(a) and 6(b) , the main frequencies turned out to be, respectively, 0.1003 and 0.0251 Hz. Therefore, the deviations between the desired and actually achieved frequencies are, respectively, 0.0003 and 0.0001 Hz. The highest frequency deviation over all 48 segments was determined to be not greater than 0.0004 Hz. It should be noted that this is a central attribute of the used verbal cueing system as by nature it yields absolute frequency adherence whereby the error diminishes the longer the segments are. This property is highly desirable in the context of these flight tests as the severity of motion sickness is mainly a function of the oscillation frequency (Ref. 22).

Questionnaires

In order to gather information from the test subjects in preparation and during the flight tests, two types of questionnaires were used. One is a preflight questionnaire intended to determine general information about the motion sickness history of the test subject in question and the second in-flight questionnaire which the test subject filled out during the flight tests in order to indicate the motion sickness state.

The preflight questionnaire is largely based on the motion sickness history questionnaire by Griffin and Howarth (Ref. 16), which was adopted and slightly extended. The original motion sickness history questionnaire was designed in order to determine the personal susceptibility to motion sickness of an individual via a total of 15 questions regarding their travel behavior on relevant modes of transport such as cars, buses, coaches, small boats, etc., the occurrence of any motion sickness symptoms during these travels and general health of the subjects. These questionnaires were adapted by translating them into German, and furthermore including a category named "Helicopters." Additionally, the category of aeroplanes was split into a category for small aircraft, for example, general aviation aircraft and commercial airplanes.

The questionnaire from Ref. 16 is supplemented with a methodology of assessing the given answers via a set of measures, regarding the

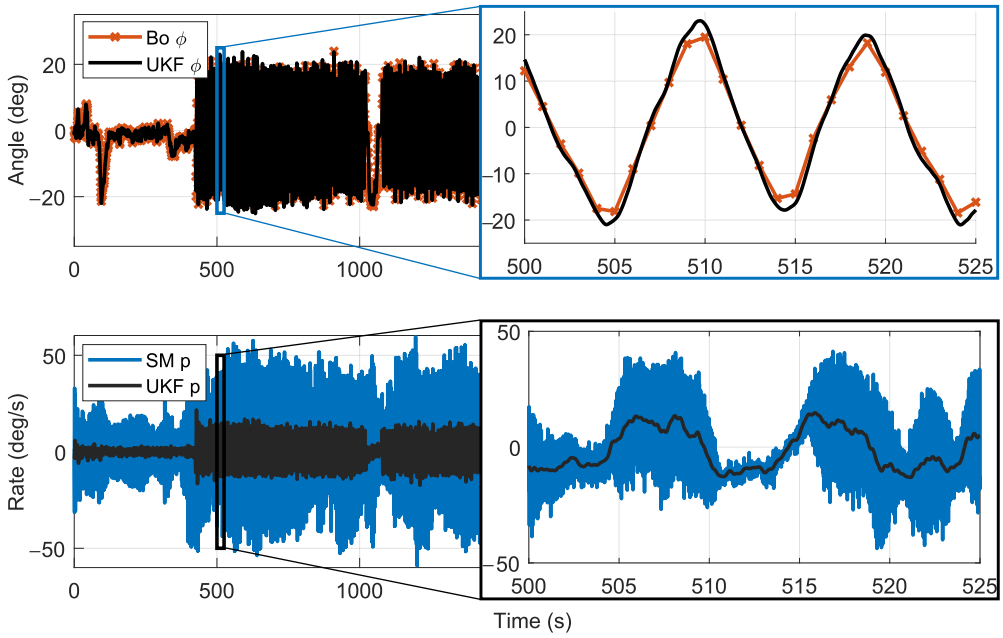

(a) Roll angle and rate

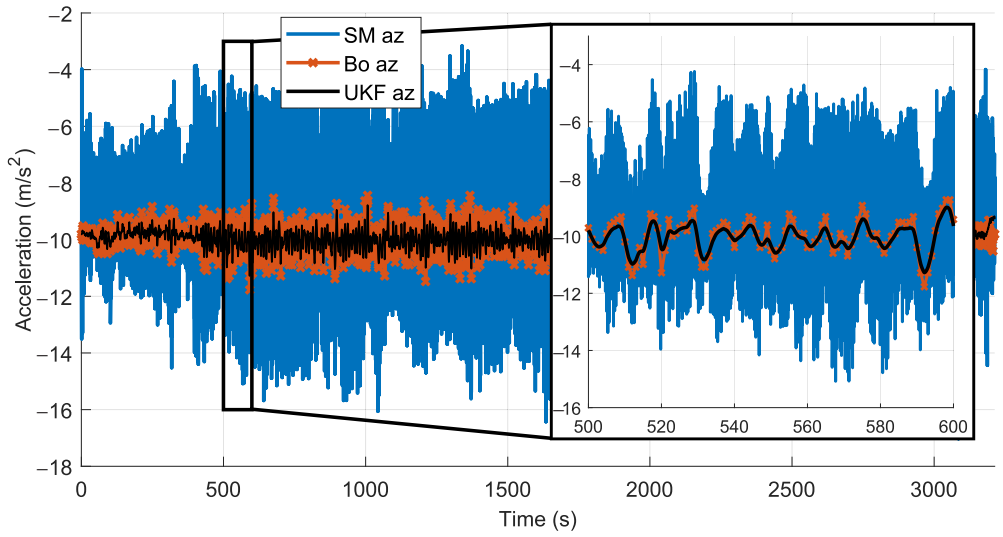

(b) Vertical acceleration

Fig. 5. Measured and estimated signals of flight 3. Smartphone measurements are in blue, G500H TXi measurement data in red, and UKF estimation data in black.

susceptibility of the given individual. For this, a number of metrics are calculated such as "Travel frequency in the past year" ($T_{(yr.)}$), "Vomiting frequency while traveling in the past year" ($V_{\text{travel(yr.)}}$), or "Illness susceptibility in transport in the past year" $I_{\text{susc.(yr.)}}$ to name a few.

These metrics were not only used for statistical analysis of the distribution of test subjects over the various flights but also to identify suitable pairs of test subjects for each flight. This was done to avoid the problem that one of the two two test subjects could get severe motion sickness and end the flight test before the other test subject would feel significant levels of motion sickness. This would diminish the "useful" flight time of the nonsick test subjects. For this reason, it was decided to pool test subjects in pairs with similar motion sickness susceptibility based on the metric "Illness susceptibility in transport in the past year" $I_{\text{susc.(yr.)}}$ determined by the preflight questionnaires. It is important to note that no statistical dependency is created with this approach as the assignment of test subjects to the flights is still random.

During the flight, the test subjects indicated their perceived motion sickness every 2 min on an in-flight questionnaire by crossing a box as shown in Fig. 7. The questionnaires used the same seven-point motion sickness scale displayed in Table 1, which was furthermore color-coded to improve the readability during flight. In total, the questionnaire consisted of four sheets, one cover for test subject identification and three sheets corresponding to one of the three 10-min test segments. The test subjects carried the questionnaire via a kneeboard. As it was feared that shifting the concentration to the kneeboard and therefore away from the outside view could cause additional motion sickness, an interval of 2 min between motion sickness indications was chosen, which was deemed to be a good compromise. The pilot nonflying supervised the test and

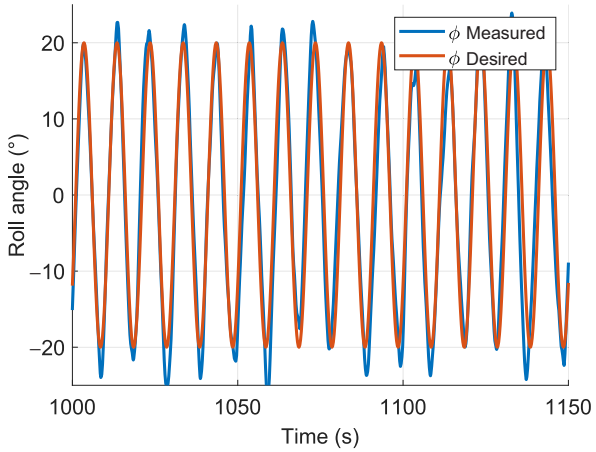

(a) Roll angle at $f = 0.1$ Hz - Extract of first segment of flight 9

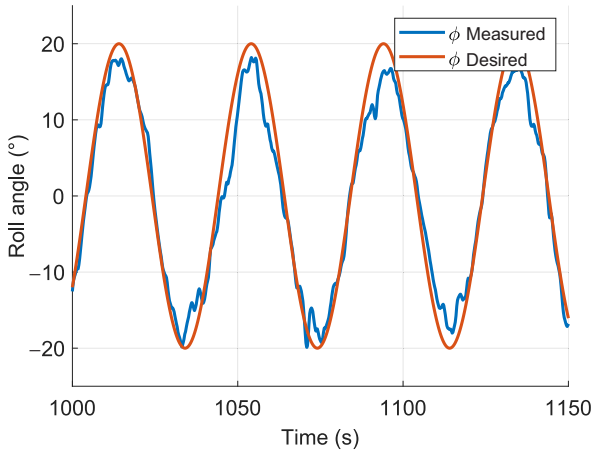

(b) Roll angle at $f = 0.025$ Hz - Extract of first segment of flight 10

Fig. 6. Two examples of resulting roll angle due to verbal pilot cueing. Desired roll in red and achieved roll angle in blue.

instructed the test subjects every 2 min to indicate their motion sickness state on the in-flight questionnaire.

Statistical Evaluation

In order to rule out variations in flight-test conditions between the different flights due to differing meteorological conditions, the manually piloted approach, or the selection and allocation of test subjects, some statistical analysis was performed. From the literature, it is expected that the main contributor to the severity of motion sickness would be the oscillation frequency (Ref. 11). To confirm this, Mann–Whitney-U and Kruskal–Wallis tests were applied to confirm that the aforementioned parameters did not favor one frequency over another.

To confirm that the test subjects were distributed such that no oscillation frequency was biased one way or another, statistical tests of age, weight, and height but also parameters from the motion sickness history questionnaire such as travel frequency, illness susceptibility, and total susceptibility were tested for equality over the three oscillation frequencies. No statistically significant differences could be found between the three oscillation frequencies and these parameters. It is, therefore, concluded that the test subjects were evenly distributed over the three oscillation frequencies with respect to their motion sickness susceptibility.

Bo105 motion sickness flight test Name:_____

1. Section, 0-10 minutes:

	0. min	2. min	4. min	6. min	8. min	10. min
0						
1						
2						
3						
4						
5						
6						

0: No symptoms	4: Mild to moderate nausea
1: Any symptoms, however slight	5: Moderate nausea but can continue
2: Mild symptoms	6: Moderate nausea and want to stop
3: Mild nausea	

Fig. 7. The in-flight questionnaire, translated from the original German questionnaire.

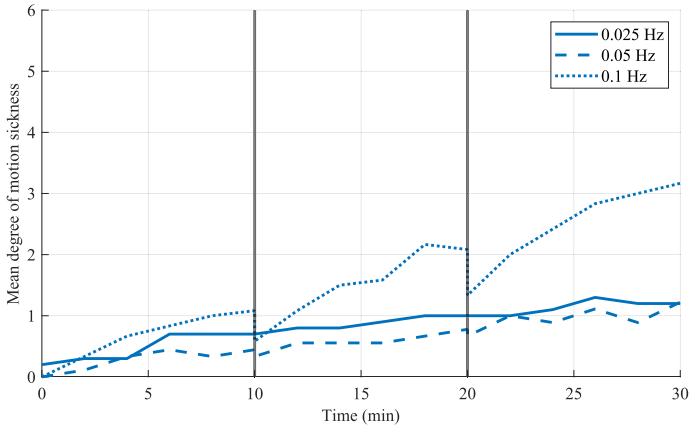

Fig. 8. Time series of the recorded mean motion sickness ratings during the test flight.

In the same manner, flight dynamics parameters such as mean and maximum roll angle, pitch angle, rotational speeds, true airspeed, wind speed, and height were analyzed. Again, the aim was to rule out an intrinsic bias of one oscillation frequency over another. No statistically

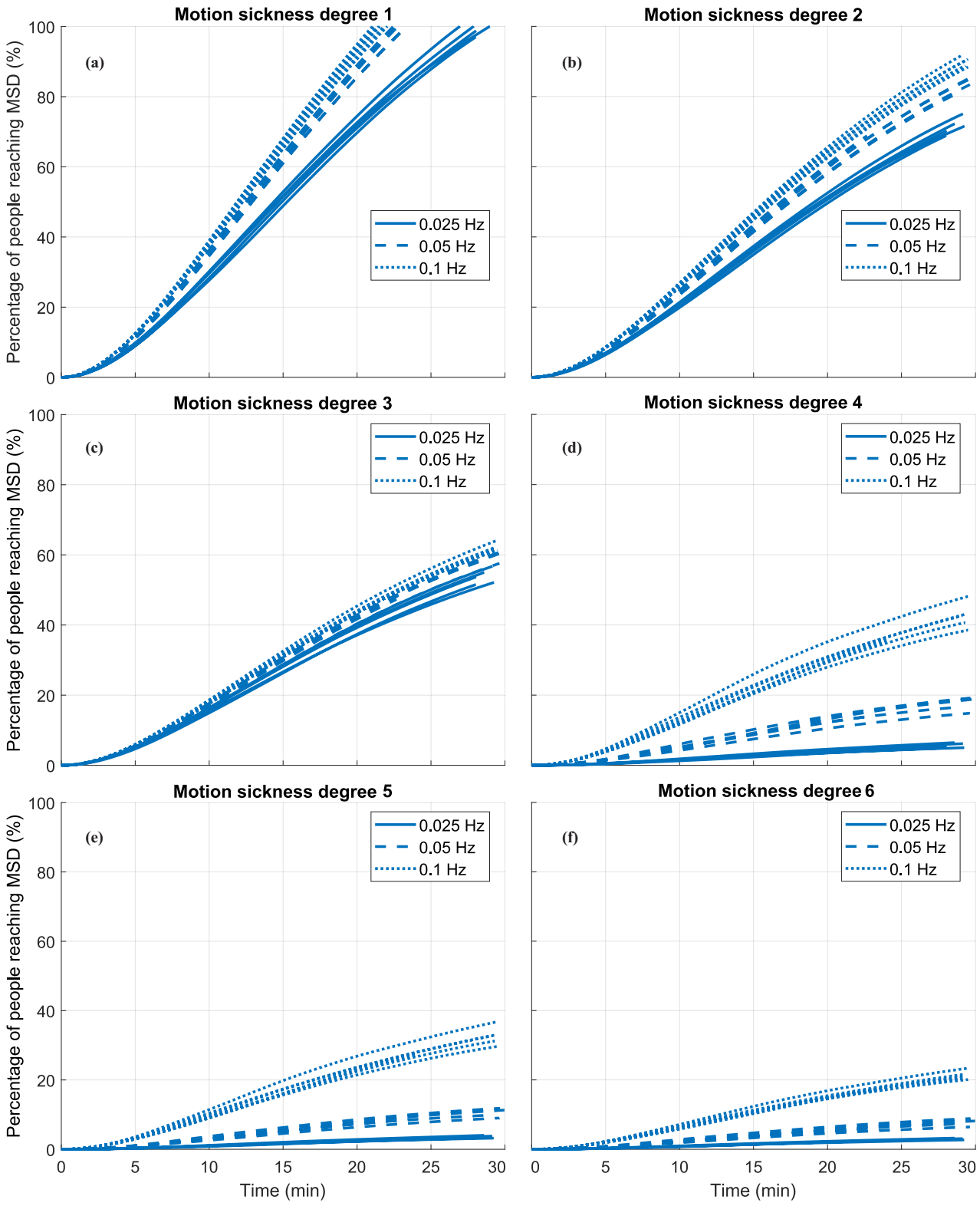

Fig. 9. Predicted percentage of people reaching one of the six motion sickness degrees, for each of the three oscillation frequencies.

significant differences could be found, except for the roll angle magnitude, which can be seen in Fig. 6, and pitch rate. Both influences stem from the manually piloted approach of the flight tests and are considered to be negligible. For example, the pitch rate difference between the three frequencies is smaller than $1\frac{^\circ}{s}$.

Flight-Test Results and Comparison to the Prediction Model

As a first step in the analysis of the flight-test results, the motion sickness ratings encountered by the test subjects during the flights are shown in Fig. 8. In this graph, the mean motion sickness of all test subjects is

plotted for the three flown frequencies. Please note that the graphs for mean motion sickness of 0.025 Hz do not start at zero as some test subjects felt slight symptoms of motion sickness because of the start and transfer of the helicopter to the first test leg. Also, the lines exhibit a small drop between each 10 min experiment leg when the helicopter completed a 180° turnaround curve as can be seen in Fig. 3. Some test subjects reported that these turnaround curves offered a small relief from motion sickness, resulting in a lower motion sickness rating. However, the general trend of the mean motion sickness curve seems to make up for this intermediate drop after a couple of minutes. Only one of the 32 test subjects flown reached a motion sickness rating of six, at the 26 min mark. Upon informing the pilot of this, the flight was aborted per test protocol.

Another flight was aborted due to nonspecified medical reasons. The data of this test subject were removed from the dataset as it could not be ruled out that the motion sickness indications of this test subject would be compromised.

From Fig. 8, it can also be seen that the reported motion sickness level for the frequencies of 0.025 and 0.05 Hz is very similar. Only the reported motion sickness degree for 0.1 Hz shows significant differences. Assuming a critical p-value of 0.05 or 5%, this intuition is confirmed by a statistical evaluation with Mann–Whitney-U tests. At the end of the flight ($t = 30$ min), there is no statistically significant difference between the mean degree of motion sickness of the 0.025 and 0.05 Hz frequencies (p-value: 0.764). In contrast, the mean degree of motion sickness of the 0.1 Hz frequency differs statistically significantly from the 0.025 Hz frequency (p-value: 0.014) and the 0.05 Hz frequency (p-value: 0.023). This leaves us with the conclusion that the 0.1 Hz frequency indeed provokes significantly more motion sickness than the other two frequencies.

To generate the predicted motion sickness, the motion data generated by the flight path reconstruction algorithm were fed into the improved Kamiji model. As presented before, this model can be parametrized with one of six different parameter sets (Ref. 8), one for each sickness level in Table 1. In total, 16 flights were performed resulting in 96 predicted motion sickness incidence rates, one for each parameter set and flight. The results can be found in Fig. 9. Several interesting observations can be made from this plot: First of all, note that the plot Fig. 9(a) reaches values *above* 100%, which is a direct consequence of the chosen model structure of the improved Kamiji model shown in Fig. 1. The introduction of the output gain K_{out}, originally introduced to enable better fitting of the data, also results in predicted motion sickness values exceeding 100%. In fact, every time $K_{\text{out}} > 1$, such a situation might occur. This problem was encountered only for motion sickness level 1. Additionally, note that some plots such as Fig. 9(d)–9(f), offer a bigger separation between the sets of curves of the three frequencies. On the other hand, all curves of motion sickness degree three Fig. 9(c) lie very close together regardless of the frequency. Also, note that some lines stop before the 30 min mark is reached, these are the flights which were aborted due to excessive motion sickness.

Probably the most interesting comparison is between the predicted and empirically determined motion sickness values. The result of this comparison for motion sickness degree four is shown in Fig. 10. In that plot, the mean of all predictions per frequency of Fig. 9(d) is shown. In comparison to the empirically determined motion sickness of the flight tests. It should be noticed that this display is different from the motion sickness ratings over time as shown in Fig. 8, as it displays the percentage of people reaching a motion sickness degree of four.

In Fig. 10, it can be seen that the simulation and the experiment generally agree. Especially in the case of the 0.1 Hz oscillation, the predicted and experiment values are very close. If one neglects the intermediate drops in motion sickness ratings of the experiment at the 10 and 20 min

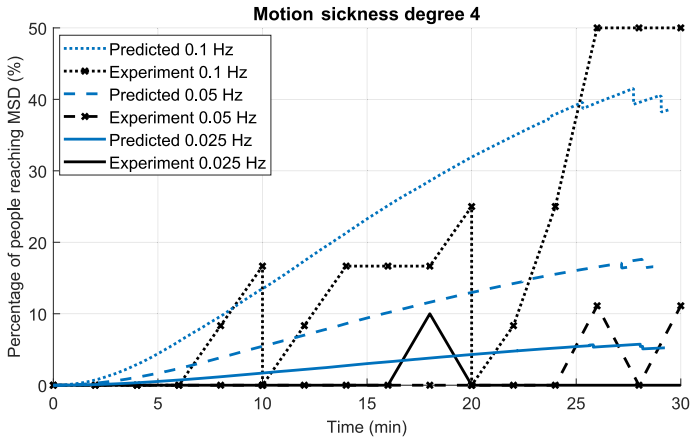

Fig. 10. Time series comparison between mean predicted (blue lines) and empirical (black lines) percentage of people reaching motion sickness degree four.

mark, the curves seem to agree even more. Again, these intermediate drops can be attributed to the turnaround curves of the flight path, and the temporary relief in motion sickness excitation these provide. In the case of 0.025 and 0.05 Hz such clear statements cannot be made because of the relatively coarse granularity of the experiment results, which is a consequence of the low number of test subjects. The motion sickness models for 0.05 Hz predict around 16% of people reaching motion sickness level four. The experiment, on the other hand, shows that roughly 11% reached this motion sickness level at the $t = 30$ min mark for that frequency. Although this means that the prediction and the experiment agree, it should also be noted that 11% is the percentage of one single test subject reaching this level of motion sickness, which is a thin basis for any statistical conclusion.

As mentioned before, a total of six different parameter sets were derived for the improved Kamiji motion sickness prediction model, one for each level of Table 1. All of these six models are compared to the results of the experiment in Fig. 11 at the $t = 30$ min mark, which is also the end of the flight test. The predictions are displayed as boxplots with a red diamond marking the mean, the red line marking the median, the box in blue marking the upper and lower quartile (25% and 75% percentile) while the whiskers in black mark the most extreme data points not considered outliers. As it is not possible to construct similar boxplots from the experimental data, only the mean is given marked by a thick black line.

As can be seen from this plot, the predictions for the percentage of people reaching a motion sickness degree of one and two are too high when compared to the experiment data. In fact, for degree one they are higher than the 100% limit of the plot. This results from the output gain K_{out} and, on the other hand, from improper data fitting. As shown in Ref. 8, a very large percentage of people reached motion sickness levels one and two resulting in an abundance of 100% values in that dataset and as a consequence improper fitting of the according models.

Similarly, inaccuracies can be observed in Fig. 11 for motion sickness levels of five and six. At these levels, the Griffin dataset offers lower data fidelity for high motion sickness values as the motions tested in the Griffin dataset were not severe enough to result in a large percentage of people reaching those high motion sickness levels. For this reason, the fitting process performed did not result in good fits of the corresponding parameter sets.

As a general observation of these flight tests, it should be noted that the number of test subjects flown on these tests is relatively low. Each frequency was only flown by around 10 test subjects. By comparison, the

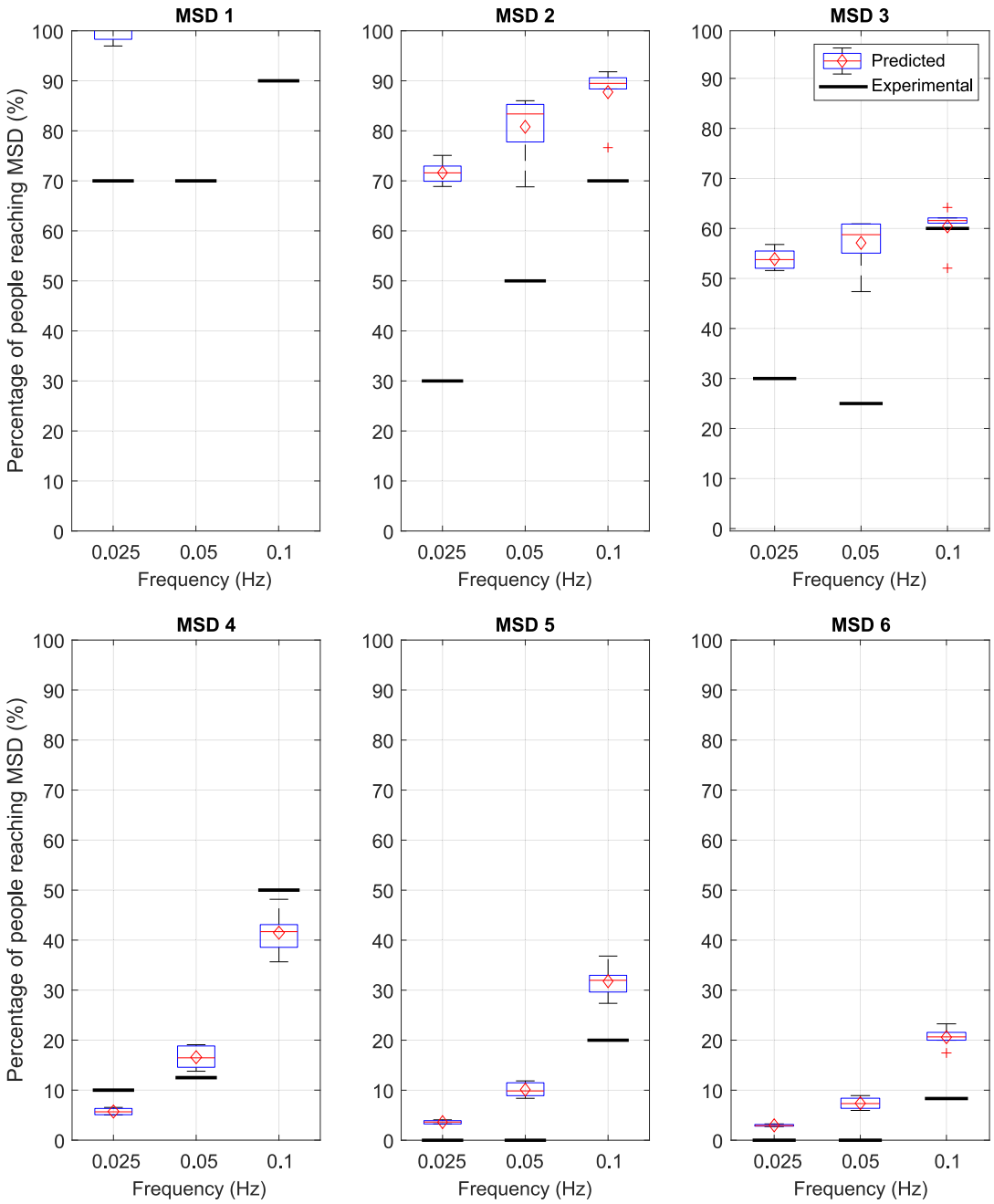

Fig. 11. Comparison of percentage of people reaching motion sickness degrees 1–6 for prediction and experiment. The predicted mean is shown as a red diamond and the experiment mean as a black thick line.

majority of the motion sickness tests conducted for the Griffin dataset contained an average of 20 test subjects per frequency (Refs. 11–15). Flight tests are, of course, prohibitively expensive if compared with simulator tests, which makes the dataset developed in this work even more valuable.

Conclusions

In support of validating the improved Kamiji motion sickness model and to generate a dataset for motion sickness, flight tests on motion sickness were carried out onboard a Bo-105 helicopter. In total 32 test subjects rated their motion sickness level during 16 flights. Several support systems were developed to enable the flight tests:

1) A flight data recording system consisting of a smartphone and the Garmin G500H TXi system digital avionics system installed in the helicopter was developed. The data of these two devices are fused with a flight path reconstruction algorithm based on an unscented Kalman filter. This approach proved to be extremely cost- and time-effective while providing good data quality for the intended purpose.

2) To enable the pilot to accurately follow the required sinusoidal roll oscillation, an auditive cueing system was devised which verbally announced desired roll angles. Data analysis showed that pilots could follow these roll oscillations with small errors. Especially the outstanding frequency adherence of the generated roll oscillation is emphasized. Workload for the pilots was high but acceptable for the duration of the flight test.

3) Questionnaires were successfully developed and used to determine motion sickness in flight and perform basic statistical data analysis on the distribution of test subjects among the different flights and the flight tests themselves.

In a final step, the motion sickness observed during the flight was compared with that predicted by the improved Kamiji model. For this, the motion data acquired throughout the flight and reconstructed by the flight path reconstruction algorithm were fed into the improved Kamiji model. By comparing the results of the prediction to the experimental results, it was determined that some parameter sets of the improved Kamiji model are better suited than others. Comparisons between the predicted motion sickness by the improved Kamiji model and the flight-test data show that especially the parameter set generating predictions for motion sickness level four seems to offer good prediction quality. As discussed in Ref. 8, this parameter set is a good compromise between data fidelity with which the parameter set was tuned and meaningful motion sickness levels. It is concluded that the improved Kamiji model with the parameter set of motion sickness level four seems to be very well suited for predicting meaningful levels of motion sickness for applications such as the design and development of new generations of autopilots, path planning algorithms, or vibration reduction systems for modern helicopters and VTOL vehicles.

References

[1]Förstberg, J., Andersson, E., and Ledin, T., "Influence of Different Conditions for Tilt Compensation on Symptoms of Motion Sickness in Tilting Trains," *Brain Research Bulletin*, Vol. 47, (5), 1998, pp. 525–535.

[2] Lawther, A., and Griffin, M. J., "Motion Sickness and Motion Characteristics of Vessels at Sea," *Ergonomics*, Vol. 31, (10), 1988, pp. 1373–1394.

[3] Vogel, H., Kohlhaas, R., and Von Baumgarten, R., "Dependence of Motion Sickness in Automobiles on the Direction of Linear Acceleration," *European Journal of Applied Physiology and Occupational Physiology*, Vol. 48, (3), 1982, pp. 399–405.

[4]Turner, M., Griffin, M. J., and Holland, I., "Airsickness and Aircraft Motion During Short-Haul Flights," *Aviation, Space, and Environmental Medicine*, Vol. 71, (12), 2000, pp. 1181–1189.

[5]Bos, J. E., MacKinnon, S. N., and Patterson, A., "Motion Sickness Symptoms in a Ship Motion Simulator: Effects of Inside, Outside, and No View," *Aviation, Space, and Environmental Medicine*, Vol. 76, (12), 2005, pp. 1111–1118.

[6]Diels, C., and Bos, J. E., "Self-Driving Carsickness," *Applied Ergonomics*, Vol. 53, 2016, pp. 374–382.

[7]Kamiji, N., Kurata, Y., Wada, T., and Doi, S., "Modeling and Validation of Carsickness Mechanism," *SICE Annual Conference 2007*, IEEE, Piscataway, NJ, 2007, pp. 1138–1143.

[8]Petit, P., "Prediction of Motion Sickness Onset for Vertical Lift Applications," *Journal of the American Helicopter Society*, **68**, 022001 (2023).

[9]Reason, J. T., and Brand, J. J., *Motion Sickness*, Academic Press, New York, NY, 1975.

[10]Bos, J., and Bles, W., "Modelling Motion Sickness and Subjective Vertical Mismatch Detailed for Vertical Motions," *Brain Research Bulletin*, Vol. 47, (5), 1998, pp. 537–542.

[11]Donohew, B. E., and Griffin, M. J., "Motion Sickness: Effect of the Frequency of Lateral Oscillation," *Aviation, Space, and Environmental Medicine*, Vol. 75, (8), 2004, pp. 649–656.

[12]Donohew, B. E., and Griffin, M. J., "Motion Sickness with Fully Roll-Compensated Lateral Oscillation: Effect of Oscillation Frequency," *Aviation, Space, and Environmental Medicine*, Vol. 80, (2), 2009, pp. 94–101.

[13]Donohew, B. E., and Griffin, M. J., "Motion Sickness with Combined Lateral and Roll Oscillation: Effect of Percentage Compensation," *Aviation, Space, and Environmental Medicine*, Vol. 81, (1), 2010, pp. 22–29.

[14]Joseph, J. A., and Griffin, M. J., "Motion Sickness from Combined Lateral and Roll Oscillation: Effect of Varying Phase Relationships," *Aviation, Space, and Environmental Medicine*, Vol. 78, (10), 2007, pp. 944–950.

[15]Beard, G. F., and Griffin, M. J., "Motion Sickness Caused by Roll-Compensated Lateral Acceleration: Effects of Centre-of-Rotation and Subject Demographics," *Proceedings of the Institution of Mechanical Engineers, Part F: Journal of Rail and Rapid Transit*, Vol. 228, (1), 2014, pp. 16–24.

[16]Griffin, M. J., and Howarth, H., "Motion Sickness History Questionnaire," ISVR Technical Report 283, Institute of Sound and Vibration Research, University of Southampton, Southampton, UK, 2000.

[17]Greiwe, D. H., Friedrich, M., and Petit, P. J., "Gaze Movements of Helicopter Pilots during Hover Flight at Different Altitudes," Proceedings of the Deutscher Luft- und Raumfahrtkongress (DLRK) 2022, Dresden, Germany, September 27–29, 2022.

[18]Ltd., G., *G500(H)/G600/G700 TXi Pilot's Guide*, January 2022. Version: 190-01717-10 - Revision M.

[19]"Minimum Operational Performance Standards (MOPS) for Strapdown Attitude and Heading Reference Systems (AHRS)," standard, RTCA, Inc., Washington DC, March 2012.

[20]Särkkä, S., "Unscented Rauch–Tung–Striebel Smoother," *IEEE Transactions on Automatic Control*, Vol. 53, (3), 2008, pp. 845–849.

[21]Wartmann, J., Wolfram, J., and Gestwa, M., "Sensor Fusion and Flight Path Reconstruction of the ACT/FHS Rotorcraft," *CEAS Aeronautical Journal*, Vol. 6, (4), 2015, pp. 529–539.

[22]ISO Central Secretary, "ISO2631-1:1997(E) Mechanical Vibration and Shock-Evaluation of Human Exposure to Whole-Body Vibration - Part 1: General Requirements," Standard, International Organization for Standardization, Geneva, Switzerland, March 1997.